This is a repository copy of *Tunable Pt nanocatalysts for the aerobic selox of cinnamyl alcohol*.

White Rose Research Online URL for this paper:
http://eprints.whiterose.ac.uk/78986/

Version: WRRO with coversheet

Article:

Universities of Leeds, Sheffield and York
http://eprints.whiterose.ac.uk/

This is an author produced version of a paper published in **Nanoscale.**

White Rose Research Online URL for this paper:

http://eprints.whiterose.ac.uk/78986/

ARTICLE TYPE

Tunable Pt nanocatalysts for the aerobic selox of cinnamyl alcohol

Lee J. Durndell,[a] Christopher M. A. Parlett,[a] Nicole S. Hondow,[b] Karen Wilson[a] and Adam F. Lee[a*]

5 The selective aerobic oxidation of cinnamyl alcohol over Pt nanoparticles has been tuning via the use of mesoporous silica supports to control their dispersion and oxidation state. High area two-dimensional SBA-15, and three-dimensional, interconnected KIT-6 silica significantly enhance Pt dispersion, and thus surface PtO_2 concentration, over that achievable via commercial low surface area silica. Selective oxidation activity scales with Pt dispersion in the order KIT-6 ≥ SBA-15 > SiO_2, evidencing surface PtO_2
10 as the active site for cinnamyl alcohol selox to cinnamaldehyde. Kinetic mapping has quantified key reaction pathways, and the importance of high O_2 partial pressures for cinnamaldehyde production.

1. Introduction

α,β-Unsaturated aldehydes are vital to a sustainable chemical economy, as they are high value intermediates/products for the
15 pharmaceutical, agrochemical and fine chemical sectors. Cinnamaldehyde for example is both a food and perfume additive,[1] conferring the flavour and aroma of cinnamon, and also serves as an insect repellent.[2] Such aldehydes are typically derived by selective oxidation of their corresponding allylic
20 alcohols. Historically stoichiometric amounts of hazardous oxidants were employed to effect such oxidations, with final product selectivity often poor and generated significant quantities of harmful waste.[3] Heterogeneous catalysts capable of such chemoselective aerobic oxidation (selox) have thus attracted great
25 interest,[4] wherein the co-existence of reactive H_2C-OH and C=C moieties is a challenge to high aldehyde selectivity.[5, 6] Consequently, a fundamental understanding of the active site and reaction network is pivotal for improving catalyst design.

Platinum group metals (PGM) are widely employed
30 heterogeneous catalysts for oxidative dehydrogenation, hydrogen transfer and oxygen insertion reactions.[7-9] Palladium has been extensively studied for the selective oxidation of allylic alcohols,[4, 10-12] wherein sophisticated in-situ/operando spectroscopic and kinetic measurements have identified surface PdO as the active
35 site responsible for crotyl and cinnamyl alcohol.[13-18] Ruthenium supported on TiO_2,[19] CeO_2,[20] Al_2O_3,[21] and hydrotalcite[22] is also effective towards allylic alcohol selox. Nanoparticulate gold also exhibits high carbonyl selectivity during alcohol selox, in the presence of an auxiliary base, and is strongly dependent on
40 nanoparticle size and metal-support interactions.[23] Biomass-derived polyfunctional alcohols, such as 5-hydroxymethyl furfural (5-HMF) can also be selectively oxidised by supported gold nanoparticles,[24] providing routes to exciting renewable polymers such as PEF (derived from 2,5-furan dicarboxylic acid,
45 FDCA).[25, 26] Bimetallic variants, such as Au/Pd[27] and Au/Pt[28] catalysts have evidenced strong synergies in alcohol selox,

resulting in enhanced activity, selectivity and lifetime.

Platinum is well-established in chemo- and enantioselective hydrogenation catalysis,[9, 29-31] including cinnamaldehyde and
50 crotonaldehyde hydrogenation wherein C=O versus C=C activation is influenced by the molecular adsorption geometry,[32] and nanoparticle size and facet termination.[33] Cinnamyl alcohol selox has also been reported over PVA-stabilised Pt colloids deposited on carbon by Prati et al,[28] however, despite exhibiting
55 high selectivity to cinnamaldehyde, their activity was extremely poor, possibly reflecting site-blocking by the polymer stabiliser.

We have previously demonstrated the importance of silica support textural properties in regulating the performance of Pd nanoparticles towards allylic alcohol selox.[34, 35] Here we
60 systematically investigate the impact of support architecture upon the structure and reactivity of analogous (naked) Pt nanoparticles, in order to identify the active catalytic site in cinnamyl alcohol selox, competing decarbonylation and hydrogenation pathways, and deactivation mechanism.

2. Experimental

2.1 Catalyst synthesis

SBA-15 synthesis.[36] Pluronic P123 (10 g) was dissolved in water (75.5 ml) and hydrochloric acid (2 M 291.5 ml) with stirring at 35
70 °C. Tetramethoxysilane (15.5 ml) was added and left for 20 h with agitation. The resulting gel was aged for 24 h at 80 °C without agitation. The solid was filtered, washed with water (1000 ml) and dried at room temp before calcination at 500 °C for 6 h in air (ramp 1 °C.min⁻¹). The resulting silica possesses hexagonally-arranged parallel pores of p6mm symmetry.

75

KIT-6 synthesis.[37] Pluronic P123 (10 g) was dissolved in water (361.6 ml), Butan-1-ol (12.3 ml) and hydrochloric acid (35 % 16.7 ml) with stirring at 35 °C. Tetramethoxysilane (15.6 ml) was added and left for 20 h with agitation. The resulting gel was aged
80 for 24 h at 80 °C without agitation. The solid was filtered, washed with water (1000 ml) and dried at room temperature before

calcination at 500 °C for 6 h in air (ramp 1 °C.min^{-1}). The resulting silica possesses a gyroidal pore architecture (Ia3 d symmetry) with interconnecting pore channels.

Pt impregnation. Mesoporous SBA-15and KIT-6 supports (2.0 g) were wetted with aqueous ammonium tetrachloroplatinate (II) solution (16 ml with precursor concentrations adjusted to achieve nominal Pt loadings of 0.05-2 wt% for SBA-15 and KIT-6 supports). Resulting slurries were stirred for 18 h at room temperature before heating to 50 °C. After 5 h, agitation ceased and the solids were left at 50 °C for 24 h to dry to a powder. These powders were calcined at 500 °C for 2 h in air (ramp 1 °Cmin^{-1}) prior to reduction at 400 °C for 2 h (ramp 10 °C.min^{-1}) under flowing hydrogen (10 ml.min^{-1}). Commercial silica (SiO$_2$) (2.0 g Sigma, 200 m^{2}g^{-1}) was likewise wetted with aqueous ammonium tetrachloroplatinate (II) solution (16 ml with varying precursor concentrations to acheive 0.05-2 wt% nominal loadings), and the slurry treated dried, calcined and reduced as above.

2.2 Characterisation

Nitrogen porosimetry was undertaken on a Quantachrome Nova 2000e porosimeter, and analysed using NovaWin software version 11. Samples were degassed at 120 °C for 2 hours prior to analysis by nitrogen adsorption at -196 °C. Adsorption/desorption isotherms were recorded for all parent and Pt-impregnated silicas. BET surface areas were calculated over the relative pressure range 0.01-0.2. Pore diameters and volumes were calculated applying the BJH method to the desorption isotherm for relative pressures >0.35. Low and wide angle XRD patterns were recorded on either a PANalytical X'pertPro diffractometer fitted with an X'celerator detector and Cu K$_\alpha$ (1.54Å) source, with calibration against a Si standard. Low angle patterns were recorded for 2θ = 0.3-8° with a step size of 0.01°. Wide angle patterns were recorded for 2θ = 20-90° with a step size of 0.02°. The Scherrer equation was used to calculate volume-averaged Pt particle sizes.

XPS was performed on a Kratos Axis HSi X-ray photoelectron spectrometer fitted with a charge neutraliser and magnetic focusing lens employing Al K$_\alpha$ monochromated radiation (1486.7 eV). Spectral fitting was performed using CasaXPS version 2.3.14. Binding energies were corrected to the Si 2p peak at 103.4 eV. Pt 4f XP spectra were fitted using a common asymmetric peak shape. Errors were estimated by varying the Shirley background-subtraction procedure across reasonable limits and re-calculating the component fits. Pt dispersions were measured via CO pulse chemisorption on a Quantachrome ChemBET 3000 system. Samples were outgassed at 150 °C under flowing He (20 ml min^{-1}) for 1 h, prior to reduction at 150 °C under flowing hydrogen (10 ml min^{-1}) for 1 h before analysis at room temperature. Note, this reduction protocol is milder than that employed during Pt impregnation, and thus does not induce additional particle sintering. A CO:Pt$_{surface}$ stoichiometry of 0.68[38, 39] was assumed, since the formation of a fully saturated monolayer is energetically unfavourable under the measurement conditions used.

SEM images were recorded on a Carl Zeiss Evo-40 SEM operating at 10 kV. Samples were supported onto aluminium stubs each backed with carbon tape. Metal loadings were determined using EDX analysis on the above instrument operating at, 25kV with a maximum current of 25nA and working distance of 9mm. High resolution (S)TEM images were recorded on an FEI Tecnai F20 field emission gun TEM operating at 200 kV equipped with a Gatan Orius SC600A CCD camera. Samples were prepared for TEM by dispersing in ethanol and drop-casting onto a copper grid coated with a continuous carbon support film (Agar Scientific Ltd). Images were analysed in ImageJ 1.41.

2.3 Cinnamyl alcohol selective oxidation

Catalyst testing was performed using Radleys Starfish carousel batch reactors on a 10 ml scale at 90 °C under atmospheric pressure of oxygen. Catalysts (50 mg) were added to reaction mixtures containing 8.4 mmol of alcohol substrate, an internal standard (mesitylene, 0.1 ml) and toluene solvent (10 ml) at 90 °C under stirring and bubbling O$_2$ (1 bar) at 5 ml min^{-1}. The absolute Pt content varied between 0.13 μmol (0.05 wt% catalysts) and 5.4 μmol (for the highest loading 2.10 wt% Pt/SiO$_2$ tested), corresponding to substrate:catalyst ratios ranging from 6.55x10^4 (0.05 wt%) down to 1.56x10^3 (2.10 wt%). Reactions were sampled periodically for kinetic profiling by off-line gas chromatography using a Varian 3900GC with 8400 autosampler fitted with a (15 m x 0.25 mm x 0.25 μm) CP-Sil5 CB column. For cinnamyl alcohol, catalytic activity towards the reaction intermediates 3-phenylpropan-1-ol, 3-phenylpropionaldehyde, cinnamic acid and cinnamaldehyde, was also measured under identical conditions to those used for cinnamyl alcohol for both high and low Pt loadings (~2 and 0.05 wt%) on all silica supports. The role of oxygen pressure was investigated under standard reaction conditions (temperature, internal standard and substrate:catalyst ratio) within a Parr Instruments stainless steel autoclave between 5 and 15 bar O$_2$ pressure; activity and selectivity were assessed after 7 h.

3. Results and discussion

3.1 Catalyst characterisation

Successful generation of the p6mm and Ia3 d silica support pore architectures for SBA-15 and KIT-6 respectively was confirmed by indexing their low angle powder X-ray diffraction (XRD) patterns (Fig. S1). The associated lattice parameters calculated from the major reflection (Table S1) are in agreement with original reports.[36, 37] As expected, nitrogen porosimetry also demonstrated type IV isotherms with type 1 hysteresis for both synthesised supports (Fig. S2), with BET surface areas and mean BJH pore sizes reported in Table S1 consistent with literature values, and evidencing narrow pore size distributions (Fig. S2). Commercial silica exhibits a type II isotherm, reflecting a disordered pore network, with a low BET surface area. Bright and dark field transmission electron microscopy (TEM) (Fig. S3) confirm the expected pore architectures in accordance with XRD and porosimetry. Complementary measurements on the Pt-doped variants showed pore arrangements and mesopore diameters comparable to their parent silicas (Fig. 1 and S4-6 and Table S2), however BET surface areas decrease of all thee supports decrease with Pt loading. The latter is greatest for SBA-15 (≤40 %) and
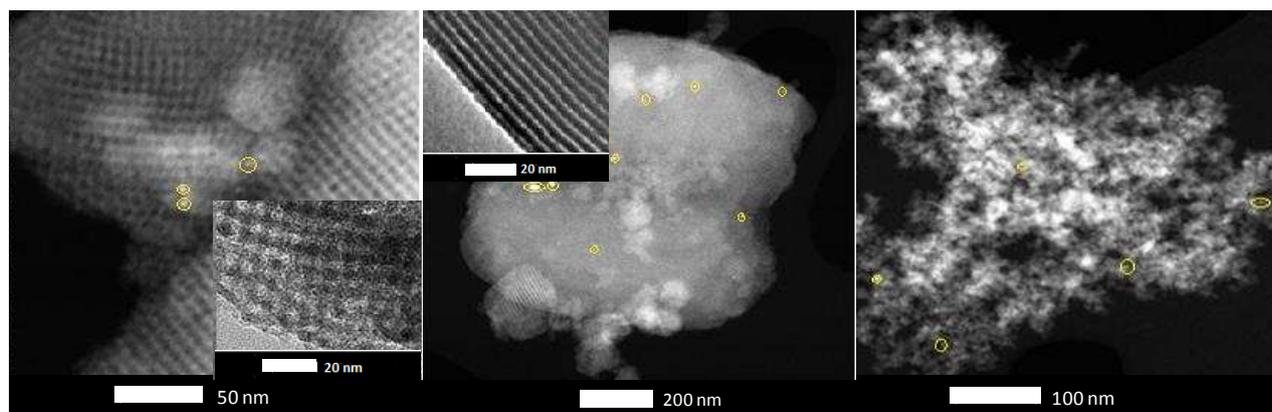
Fig. 1 Dark field STEM images of (left) 0.06 wt% Pt/KIT-6; (centre) 0.06 wt% Pt/SBA-15; and (right) 0.05 wt% Pt/SiO₂ catalysts. Yellow circles highlight dispersed Pt nanoparticles; insets show bright-field TEM images of parent SBA-15 and KIT-6 mesoporous silicas

KIT-6 (≤30 %), and likely arises from partial pore blockage, with the interconnecting pores of KIT-6 mitigating this effect. The smaller decrease observed for the commercial silica is consistent with Pt nanoparticles residing predominantly over its proportionately larger external surface area. Platinum nanoparticle dispersion increases with diminishing loading as shown in Fig. 2a and Table S2. The derived Pt nanoparticle sizes are in good agreement with those calculated from the Scherrer equation from the corresponding XRD patterns for loadings >0.5 wt% and show a dramatic decrease in size from 15 nm (2 wt%) to 2.7 nm (0.05 wt%) for the Pt/SBA-15 series. Only fcc Pt metal reflections were observed by wide angle XRD for all supports. Platinum dispersion was sensitive to the silica support, with mesoporous silicas demonstrating increased metal dispersions of 71% (SBA-15) and 80% (KIT-6) relative to 44% for the commercial silica at comparable 0.1 wt% loadings. These differences were reflected in dramatically different degrees of surface oxidation as measured by XPS (Fig. S8 and S9), resulting in a linear correlation between surface oxide concentration state and dispersion (Fig. 2b) as we previously observed for Pt/Al₂O₃,[40] and Pd/silica and Pd/Al₂O₃ analogues.[34, 35, 41] In all cases, the Pt $4f_{7/2}$ oxide binding energies (74.3 eV) were consistent with PtO₂ and not PtO, in accordance with Ono et al.[42] All three supports exhibit similar loading versus oxidation state relations, precisely as expected since silica is a weakly-interacting support. Hence, in this instance, Pt oxidation state is solely determined by nanoparticle dispersion, the latter a function of silica surface area. The distribution of PtO₂ was explored via two different X-ray excitation sources (Mg versus Al K_α) to provide different Pt 4f photoelectron sampling depths, as described in the ESI. The results indicate a metal core-oxide shell structure, as may be anticipated given the slow diffusion of oxygen into the bulk of metals, which typically follows Mott-Cabrera kinetics,[43, 44] i.e. rapid formation of a passivating surface oxide followed by slow diffusion into the underlying core. For a 0.1 wt% Pt/SiO₂ catalyst, the PtO₂ film thickness is estimated at ~0.8 nm (≡ 3 layers of crystalline PtO₂).

3.2 Cinnamyl alcohol selective oxidation

Cinnamyl alcohol (CinnOH) aerobic selox was explored over our three Pt/SiO₂ catalyst families via reaction profiling (Fig. S10).
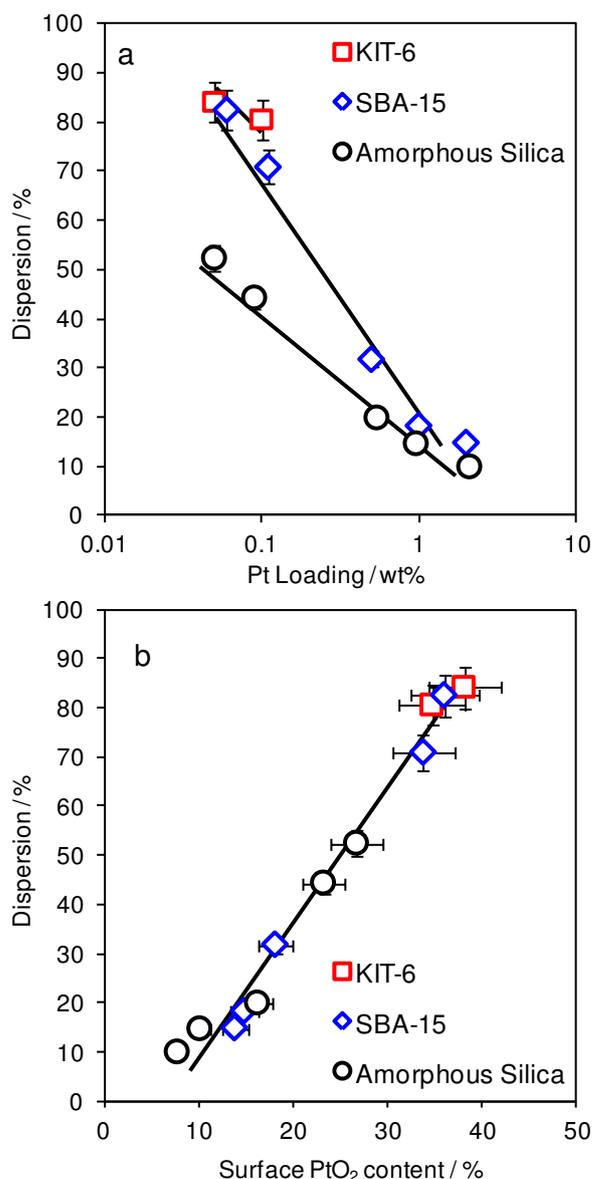

Fig. 2 Influence of Pt loading and support architecture on (a) Pt dispersion; and (b) surface PtO₂ concentration

Control experiments evidenced negligible conversion in the absence of supported platinum, with hot filtration tests showing no detectable platinum leaching, demonstrating purely heterogeneous platinum catalysed selox. Initial selox rates are inversely proportional to Pt loading for all supports (Fig. 3a), replicating prior observations for Pd impregnated silicas,[34] albeit with lower activity per gram of metal. Mesoporous silica confer significantly higher selox activity than their commercial analogue, with Pt/KIT-6 ≅ Pt/SBA-15 > Pt/SiO₂. Quantification of the PtO₂ content of each catalyst, and corresponding activity, reveals a hitherto undiscovered linear relationship between the two (Fig. 3b). This striking finding strongly suggests that PtO₂ is the active site in platinum catalysed cinnamyl alcohol selox, precisely as we recently demonstrated for the analogous palladium catalysis, and underpins the observed rates in Fig 3a. We postulate that the high surface area silicas favour highly

dispersed Pt nanoparticles which undergo preferential oxidation to minimise their surface energies, and are thus more active than larger Pt nanoparticles present in metallic form over the low surface area silica. In order to assess the potential significance of support interactions, we have also examined the reactivity of platinum deposited on CeO₂ and ZrO₂, respective reducible and Lewis acidic metal oxide supports (Fig. S11). The results show that under our mild reaction conditions, the principal factor influencing Pt catalysed alcohol selox is not the chemical nature of the oxide support, but rather the support surface area, which influences the platinum dispersion as described above, and thus degree of oxidation, which in turn controls activity. This is evident from Fig. 3b, wherein the structure-reactivity properties of 0.1 wt% Pt/ZrO₂ (100 m².g⁻¹) and 0.1 wt% Pt/CeO₂ (5 m².g⁻¹) catalysts both fit perfectly on the line derived for weakly-interacting silica supports, while their corresponding selectivity profiles are almost identical to that of 0.1 wt% Pt/SiO₂ (Fig. S12) implicating a common reaction mechanism and active site.

The preceding hypothesis was tested by comparing the turnover frequencies (TOFs) for cinnamyl alcohol selox per Pt^0 or Pt^{4+} site. In the absence of mass-transport limitations, identification of the true active species should yield a constant TOF independent of silica support or Pt loading. Fig. 4 shows that normalisation to surface Pt metal results in a decreasing TOF with metal loading. In contrast, normalisation to surface PtO₂ reveals a constant TOF, precisely as expected for an oxide active site. Surprisingly, the resultant TOF of 6,000 h⁻¹ is in excellent agreement with that derived for Pd/silicas of 5,800 h⁻¹.[35,34] This finding contrasts with earlier studies, which erroneously compared similar loading Pt and Pd catalysts possessing different dispersions, and hence unfairly concluded that palladium was far superior to platinum.[45,46]
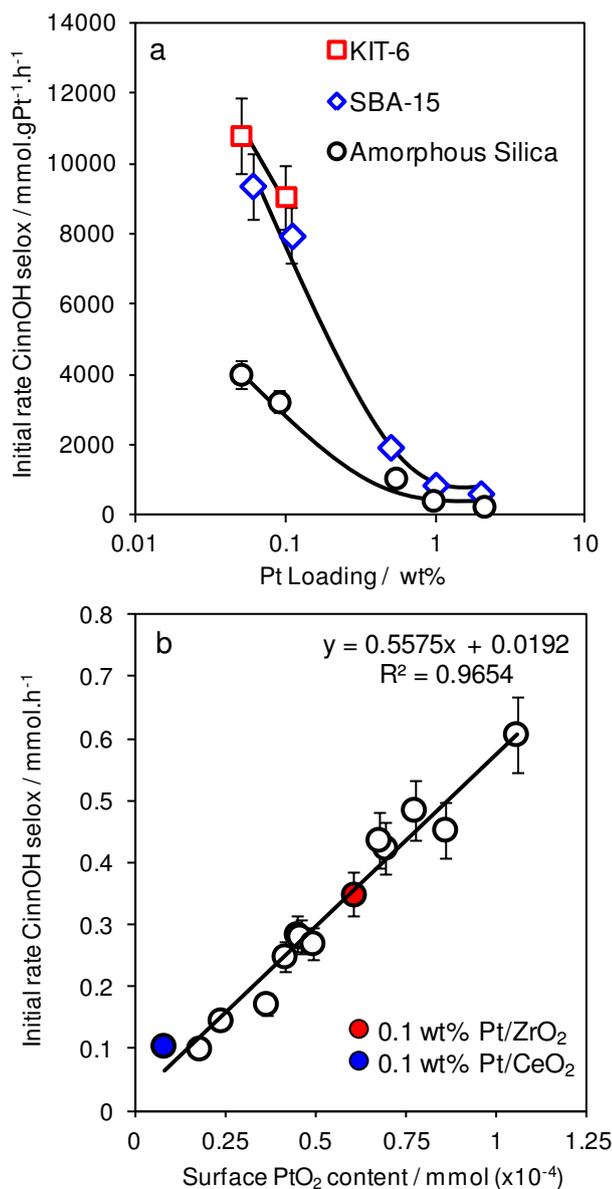

Fig. 3 Initial rate dependence of cinnamyl alcohol selox on (a) Pt loading and support architecture and (b) surface PtO₂ concentration
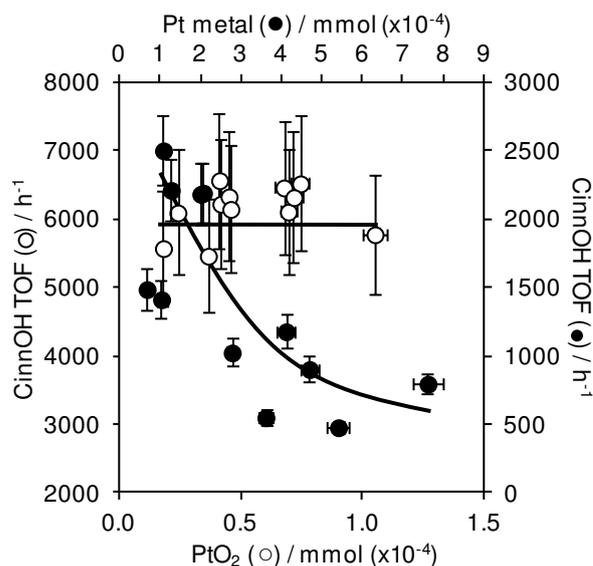

Fig. 4 TOF normalised to surface Pt or PtO₂ concentration

Selectivity towards the desired cinnamaldehyde oxidation product is critical to the commercial application of selox catalysts. A representative selectivity profile shown in Fig. 5 highlights the high initial selectivity to cinnamaldehyde (~65 %), which however falls to only 25 % during reaction, due to
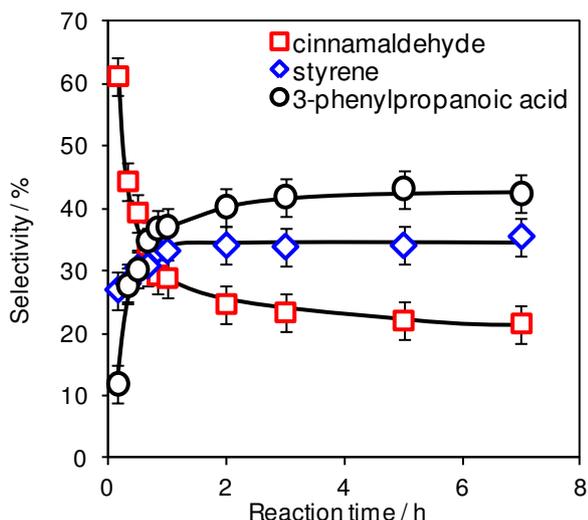
Fig. 5 Selectivity profile for a 0.05 wt% Pt/SiO$_2$ catalyst

undesired 3-phenylpropanoic acid and styrene production. The carboxylic acid likely forms via hydrogenation of the C=C function and over-oxidation of the alcohol function, whereas styrene must form via hydrogenolysis of the C-C bond.

Comparison with Pd/silica analogues[35,34] reveals significantly higher levels of C=C hydrogenation over platinum, consistent with the latter's performance in liquid phase alkene hydrogenation.[47] Styrene formation during cinnamyl alcohol selox over Pd/silicas is indicative of the presence of palladium metal,[35] and by analogy, may reflect in-situ reduction of surface PtO2 under our reaction conditions. In order to test whether hydrogenation side-reactions were indeed favoured by metallic platinum, the ratio of cinnamaldehyde:3-phenylpropanoic acid was determined as a function of surface Pt^0 concentration across all three Pt/silica families. Fig. 6 confirms this postulate, with selectivity towards hydrogenation versus oxidation products increasing with the degree of platinum surface reduction. Further
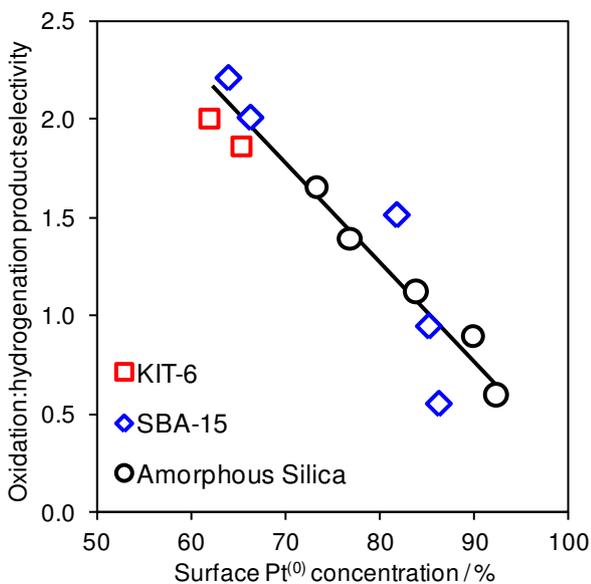
Fig. 6 Detrimental impact of surface Pt$^{(0)}$ on selectivity to oxidation (cinnamaldehyde) versus hydrogenation (3-phenylpropanoic acid)

evidence for the link was provided by in-situ pre-reduction of the 0.05 wt% Pt/SiO$_2$ catalyst, which lowered the initial cinnamaldehyde selectivity by 12 % (Fig. S13). A further demonstration that PtO2 is essential for cinnamyl alcohol selox was provided by increasing the oxygen pressure. Fig. 7 shows that increasing the p$_{O2}$ from 1 to 15 bar enhanced cinnamyl alcohol conversion by 45 %, and the ratio of oxidation:hydrogenation products from 0.65 to 1.1. XPS of fresh and spent catalysts shown in Fig. 8 confirms that this enhanced selox performance reflects stabilisation of surface PtO$_2$ under higher O$_2$ pressures. In-situ PtO$_2$ reduction induced by cinnamyl alcohol lowers the surface oxide content from 20.5 % during the early stages of reaction, to only 5 % after 24 h under 1 bar O$_2$. By comparison, 13 % PtO$_2$ remains after 24 h reaction under 10 bar O$_2$. The requirement for elevated oxygen pressures to achieve comparable cinnamaldehyde yields over Pt/silicas as obtained for Pd/silicas may originate in part from the lower oxygen sticking probability over platinum.[48]
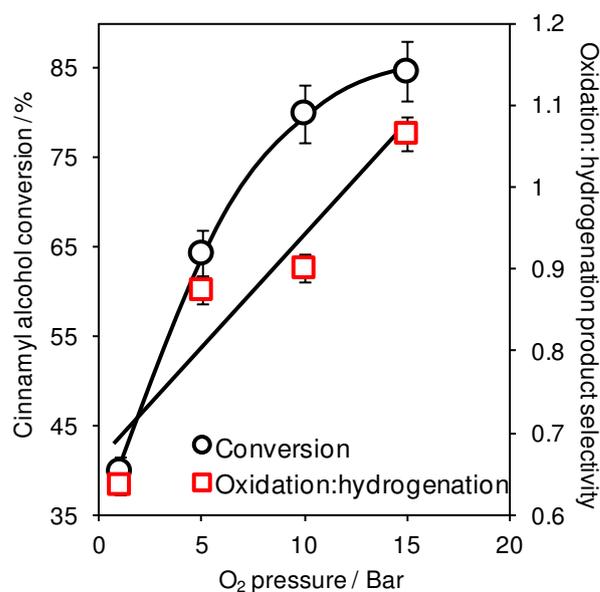

Fig. 7 Influence of O$_2$ reaction pressure on cinnamyl alcohol conversion and oxidation:hydrogenation product selectivity for a 0.05 wt% Pt/SiO$_2$ catalyst
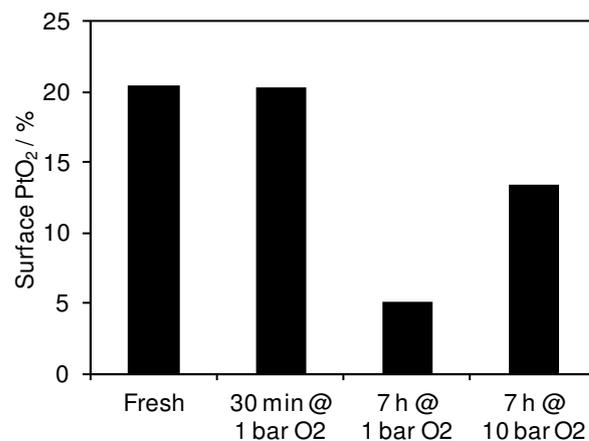

Fig. 8 Influence of cinnamyl alcohol selox reaction time and O$_2$ pressure on surface PtO$_2$ concentration for a 0.05 wt% Pt/SiO$_2$ catalyst
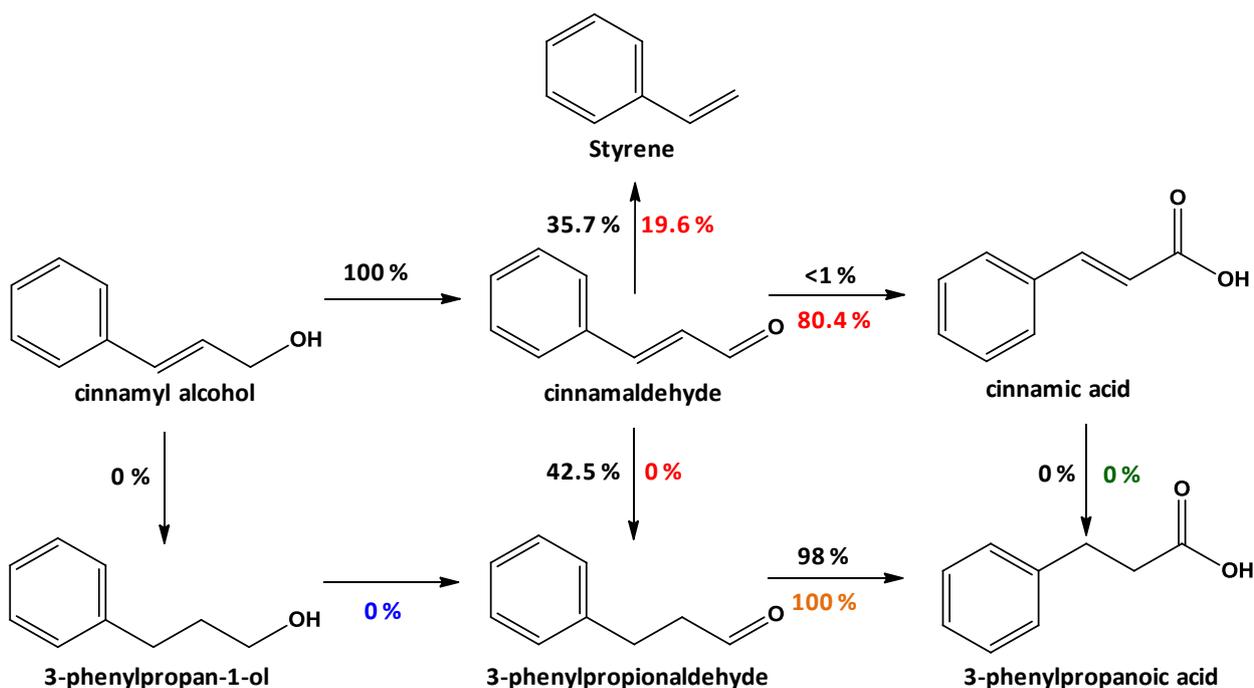
Scheme 1 Reaction network for cinnamyl alcohol selox over a 0.05 wt% Pt/SBA-15 catalyst at 90 °C, 8.4 mmol substrate and 1 bar O_2. Starting substrate colour key: black = cinnamyl alcohol; red = cinnamaldehyde; green = cinnamic acid; blue = 3-phenylpropan-1-ol; and orange 3-phenylpropionaldehyde.

Further insight into the product selectivities was obtained by studying the reactivity of various potential intermediates under standard selox conditions over a 0.05 wt% Pt/SBA-15 catalyst. The results are summarised in Scheme 1 after 7 h of reaction; the values reported represent the percentage of each reactant that follows a particular pathway. Considering cinnamyl alcohol, the first step is always oxidation to cinnamaldehyde, with no direct C=C hydrogenation of the alcohol. However, the cinnamaldehyde product is unstable with respect to decarbonylation (to styrene) and hydrogenation (to 3-phenylpropionaldehyde), leaving only 22 % of reactively formed cinnamaldehyde intact. The 3-phenylpropionaldehyde intermediate is itself extremely unstable with respect to subsequent oxidation to the corresponding 3-phenylpropanoic acid. Interestingly, reactively-formed cinnamaldehyde does not undergo over-oxidation to cinnamic acid under our conditions, presumably because surface hydrogen co-liberated during its formation from cinnamyl alcohol promotes competing hydrogenolysis/hydrogenation pathways. In contrast, when cinnamaldehyde is selected as the starting material, over-oxidation to cinnamic acid is the dominant pathway, reflecting the absence of surface hydrogen. Cinnamic acid is stable with respect to decarboxylation to styrene, and hydrogenation to 3-phenylpropanoic acid, as expected for such a highly conjugated molecule under mild oxidation conditions. The high stability of C-H bonds adjacent to the hydroxyl function in 3-phenyl propan-1-ol renders this saturated alcohol inert under our conditions.[49]

The preceding experiments enable us to map out the reaction pathways for cinnamyl alcohol. These highlight that while platinum is an effective oxidation catalyst, facilitating both oxidative dehydrogenation and oxygen insertion reactions to form cinnamaldehyde and cinnamic acid, it also promotes hydrogen transfer reactions with high efficiency and the attendant loss of molecular functionality. This contrasts with palladium based catalysts, wherein higher selectivity to cinnamaldehyde is obtained, which we attribute to the higher stability of palladium oxide versus metal. In order to evaluate the wider applicability of our Pt/silica catalysts in the aerobic selox of unsaturated oxyenates, 0.05 wt% Pt/SBA-15 was screened against a range of alcohols, aldehydes, and ketones (Table 1). The results demonstrate promising activity for the oxidation of unsaturated primary aldehydes and alcohols, such as crotonaldehyde, hydrocinnamaldehyde, benzyl alcohol, 1-phenyl ethanol and trans-2-methyl-3-phenyl-2-propen-1-ol, while secondary alcohols and ketones proved less reactive under our mild reaction conditions. This highlights the importance of proximity between aromatic/allyl functions and the terminal OH/HCO group as previously observed for a Pt/graphite catalyst.[49] We are currently developing bimetallic M-Pt catalysts to fine tune the rates of oxidation versus hydrogenation, to maximise activity and selectivity to allylic aldehydes and acids.

4. Conclusions

Silica-supported Pt nanoparticles are active for the liquid phase selective aerobic oxidation of cinnamyl alcohol to cinnamaldehyde at low temperature and ambient oxygen pressure. Catalyst activity is a strong function of platinum dispersion, which in turn controls the concentration of surface PtO_2, the active site responsible for the desired selox chemistry. High area, mesoporous silicas enhance platinum dispersion and thus PtO_2 content, conferring superior activity to low area silica. Selectivity reflects a delicate balance of oxidation and competing hydrogenation/hydrogenolysis pathways, the latter driven by in-situ hydrogen production and associated nanoparticle reduction.

Table 1. Selox performance of 0.05 wt% Pt/SBA-15 towards unsaturated and saturated oxygenates at 90 °C[a]

Substrate	Primary product	C[b] / %	S[c] / %
Crotonaldehyde	Crotonic Acid	27	66
Trans-hexen-1-ol	Trans-hex-3-enal	11	72
Cinnamyl alcohol	Hydrocinnamic acid	38	42
Cinnamaldehyde	Cinnamic Acid	31	80
Hydrocinnamaldehyde	Hydrocinnamic acid	58	95
Hydrocinnamyl alcohol	n/a	0	0
Benzyl alcohol	Benzaldehyde	30	92
1-Phenyl ethanol	Acetophenone	25	100
Trans-2-methyl-3-phenyl-2-propen-1-ol	(E)-2-methyl-3-phenylacrylaldehyde	13	68
Geraniol	(E)-3,7-dimethylocta-2,6-dienal	6	100
3-Penten-2-ol	(E)-Pent-3-en-2-one	7	72
3-Methyl-3-buten-1-ol	n/a	0	0
Linalool	Isomers	3	100
(E)-4-Phenylbut-3-en-2-one	n/a	0	0
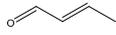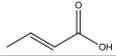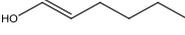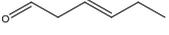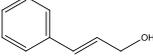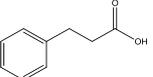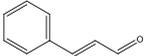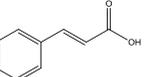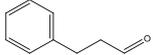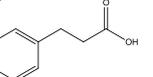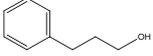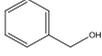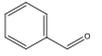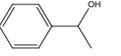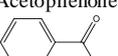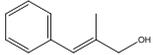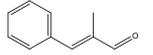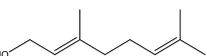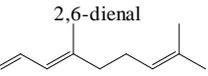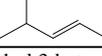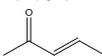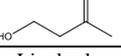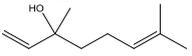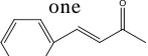
[a] 0.05 g catalyst and 8.4 mmol substrate (substrate:catalyst = 65,500); 1 bar flowing O_2 at 3 ml.min^{-1}; [b]Conversion and [c]Selectivity after 7 h.

Acknowledgements

Notes and references

[a]Cardiff Catalysis Institute, School of Chemistry, Cardiff University, Cardiff CF10 3AT, UK. Fax: 44 2920 874030; Tel: 44 2920 874778; E-mail: leeaf@cardiff.ac.uk
[b]Institute for Materials Research, School of Process, Environmental and Materials Engineering, University of Leeds, Leeds LS2 9JT, UK.

† Electronic Supplementary Information (ESI) available: Full details of catalyst synthesis, characterisation and testing. See DOI: 10.1039/b000000x/

1. J. Cocchiara, C. S. Letizia, J. Lalko, A. Lapczynski and A. M. Api, Food Chem. Toxicol., 2005, **43**, 867-923.
2. S. S. Cheng, J. Y. Liu, K. H. Tsai, W. J. Chen and S. T. Chang, J. Agric. Food Chem., 2004, **52**, 4395-4400.
3. J. H. Clark, Green Chem., 1999, **1**, 1-8.
4. C. P. Vinod, K. Wilson and A. F. Lee, J. Chem. Technol. Biotechnol., 2011, **86**, 161-171.
5. P. Sautet and F. Delbecq, J. Catal., 1995, **152**, 217-236.
6. P. G. N. Mertens, J. Wahlen, X. Ye, H. Poelman and D. E. Vos, Catal. Lett., 2007, **118**, 15-21.
7. T. Mallat and A. Baiker, Catal. Today, 1995, **24**, 143-150.
8. C. Keresszegi, T. Burgi, T. Mallat and A. Baiker, J. Catal., 2002, **211**, 244-251.
9. G. Kyriakou, S. K. Beaumont and R. M. Lambert, Langmuir, 2011, **27**, 9687-9695.
10. Y. T. Chen, Z. Guo, T. Chen and Y. H. Yang, J. Catal., 2010, **275**, 11-24.
11. W. B. Hou, N. A. Dehm and R. W. J. Scott, J. Catal., 2008, **253**, 22-27.
12. T. Yasu-eda, R. Se-ike, N. O. Ikenaga, T. Miyake and T. Suzuki, J. Mol. Catal. A: Chem., 2009, **306**, 136-142.
13. A. F. Lee, C. V. Ellis, J. N. Naughton, M. A. Newton, C. M. A. Parlett and K. Wilson, J. Am. Chem. Soc., 2011, **133**, 5724-5727.
14. C. V. Gaskell, C. M. A. Parlett, M. A. Newton, K. Wilson and A. F. Lee, ACS Catal., 2012, **2**, 2242-2246.
15. A. F. Lee, J. N. Naughton, Z. Liu and K. Wilson, ACS Catal., 2012, **2**, 2235-2241.
16. C. M. A. Parlett, C. V. Gaskell, J. N. Naughton, M. A. Newton, K. Wilson and A. F. Lee, Catal. Today, http://dx.doi.org/10.1016/j.cattod.2012.1008.1022.
17. A. F. Lee, S. F. J. Hackett, J. S. J. Hargreaves and K. Wilson, Green Chemistry, 2006, **8**, 549-555.
18. A. F. Lee and K. Wilson, Green Chemistry, 2004, **6**, 37-42.
19. A. Köckritz, M. Sebek, A. Dittmar, J. Radnik, A. Brückner, U. Bentrup, M. M. Pohl, H. Hugl and W. Mägerlein, J. Mol. Catal. A: Chem., 2006, **246**, 85-99.
20. H. B. Ji, T. Mizugaki, K. Ebitani and K. Kaneda, Tetrahedron Lett., 2002, **43**, 7179-7183.
21. K. Yamaguchi and N. Mizuno, Angew. Chem.-Int. Edit., 2002, **41**, 4538-4542.
22. T. Matsushita, K. Ebitani and K. Kaneda, Chem. Commun., 1999, 265-266.
23. G. J. Hutchings, Chem. Commun., 2008, 1148-1164.

24. S. E. Davis, B. N. Zope and R. J. Davis, Green Chem., 2012, **14**, 143-147.

25. S. E. Davis, M. S. Ide and R. J. Davis, Green Chem., 2013, **15**, 17-45.

26. J. J. Bozell and G. R. Petersen, Green Chemistry, 2010, **12**, 539-554.

27. J. A. Lopez-Sanchez, N. Dimitratos, N. Glanville, L. Kesavan, C. Hammond, J. K. Edwards, A. F. Carley, C. J. Kiely and G. J. Hutchings, Appl. Catal., A, 2011, **391**, 400-406.

28. N. Dimitratos, A. Villa, D. Wang, F. Porta, D. Su and L. Prati, J. Catal., 2006, **244**, 113-121.

29. T. Mallat, E. Orglmeister and A. Baiker, Chem. Rev., 2007, **107**, 4863-4890.

30. M. S. Ide, B. Hao, M. Neurock and R. J. Davis, ACS Catal., 2012, **2**, 671-683.

31. M. Shirai, T. Tanaka and M. Arai, J. Mol. Catal. A: Chem., 2001, **168**, 99-103.

32. A. J. Urquhart, F. J. Williams, O. P. H. Vaughan, R. L. Cropley and R. M. Lambert, Chemical Communications, 2005, **0**, 1977-1979.

33. W. O. Oduro, N. Cailuo, K. M. Yu, H. Yang and S. C. Tsang, Phys. Chem. Chem. Phys., 2011, **13**, 2590-2602.

34. C. M. A. Parlett, D. W. Bruce, N. S. Hondow, A. F. Lee and K. Wilson, ACS Catal., 2011, **1**, 636-640.

35. C. M. A. Parlett, D. W. Bruce, N. S. Hondow, M. A. Newton, A. F. Lee and K. Wilson, ChemCatChem, 10.1002/cctc.201200301.

36. D. Zhao, J. Feng, Q. Huo, N. Melosh, G. H. Fredrickson, B. F. Chmelka and G. D. Stucky, Science, 1998, **279**, 548-552.

37. F. Kleitz, S. Hei Choi and R. Ryoo, Chem. Commun., 2003, 2136-2137.

38. R. Chen, Z. Chen, B. Ma, X. Hao, N. Kapur, J. Hyun, K. Cho and B. Shan, Computational and Theoretical Chemistry, 2012, **987**, 77-83.

39. S. R. Longwitz, J. Schnadt, E. K. Vestergaard, R. T. Vang, E. Laegsgaard, I. Stensgaard, H. Brune and F. Besenbacher, Journal of Physical Chemistry B, 2004, **108**, 14497-14502.

40. A. F. Lee, K. Wilson, R. M. Lambert, C. P. Hubbard, R. G. Hurley, R. W. McCabe and H. S. Gandhi, J Catal, 1999, **184**, 491-498.

41. S. E. J. Hackett, R. M. Brydson, M. H. Gass, I. Harvey, A. D. Newman, K. Wilson and A. F. Lee, Angew. Chem.-Int. Edit., 2007, **46**, 8593-8596.

42. L. K. Ono, B. Yuan, H. Heinrich and B. R. Cuenya, The Journal of Physical Chemistry C, 2010, **114**, 22119-22133.

43. N. Cabrera and N. F. Mott, Reports on Progress in Physics, 1949, **12**, 163.

44. C. V. Gaskell, C. M. A. Parlett, M. A. Newton, K. Wilson and A. F. Lee, Acs Catal, 2012, **2**, 2242-2246.

45. P. Gallezot, Catal. Today, 1997, **37**, 405-418.

46. R. Garcia, M. Besson and P. Gallezot, Appl. Catal., A, 1995, **127**, 165-176.

47. I. Pálinkó, Appl. Catal., A, 1995, **126**, 39-49.

48. Å. Johansson, M. Försth and A. Rosén, Surface Science, 2003, **529**, 247-266.

49. A. F. Lee, J. J. Gee and H. J. Theyers, Green Chemistry, 2000, **2**, 279-282.